Path-integral method for the source apportionment of photochemical pollutants

A. M. Dunker[1]

[1]{A. M. Dunker, LLC, Bloomfield Hills, Michigan, USA}

Correspondence to: A. M. Dunker (amdunker@gmail.com)

Abstract

A new, path-integral method is presented for apportioning the concentrations of pollutants predicted by a photochemical model to emissions from different sources. A novel feature of the method is that it can apportion the difference in a species concentration between two simulations. For example, the anthropogenic ozone increment, which is the difference between a simulation with all emissions present and another simulation with only the background (e.g., biogenic) emissions included, can be allocated to the anthropogenic emission sources. The method is based on an existing, exact mathematical equation. This equation is applied to relate the concentration difference between simulations to line or path integrals of first-order sensitivity coefficients. The sensitivities describe the effects of changing the emissions and are accurately calculated by the decoupled direct method. The path represents a continuous variation of emissions between the two simulations, and each path can be viewed as a separate emission-control strategy. The method does not require auxiliary assumptions, e.g., whether ozone formation is limited by the availability of volatile organic compounds (VOC's) or nitrogen oxides (NO_x), and can be used for all the species predicted by the model. A simplified configuration of the Comprehensive Air Quality Model with Extensions is used to evaluate the accuracy of different numerical integration procedures and the dependence of the source contributions on the path. A Gauss-Legendre formula using 3 or 4 points along the path gives good accuracy for apportioning the anthropogenic increments of ozone, nitrogen dioxide, formaldehyde, and nitric acid. Source contributions to these increments were obtained for paths representing proportional control of all anthropogenic emissions together, control of NO_x emissions before VOC emissions, and control of VOC emissions before NO_x emissions. There

are similarities in the source contributions from the three paths but also differences due to the different chemical regimes resulting from the emission-control strategies.

1 Introduction

The goal of source apportionment is to determine, quantitatively, how much different emission sources contribute to a given pollutant concentration. Source apportionment is thus a useful tool in developing efficient strategies to meet air quality standards by identifying the most important sources. If emissions are involved in only linear processes between where they are emitted and where they impact a receptor location, the concentration of the pollutant at the receptor is the sum of independent contributions from the individual emission sources. For example, one can define a tracer for each source of primary, unreactive particulate matter (PM) in an air quality model such that the sum of the tracer concentrations is the total primary PM concentration and the tracer concentrations form the source apportionment. However, if a secondary pollutant is formed by nonlinear chemical reactions, source apportionment is more complicated and, indeed, there is no unique apportionment.

Reflecting this non-uniqueness, a number of approaches have been developed for source apportionment of secondary pollutants. The simplest approach is source removal or the brute force method. Simulations with and without a particular source are compared, and the changes in predicted concentrations are assigned to emissions from that source (Marmur et al., 2006; Tong and Mauzerall, 2008; Wang et al., 2009; Zhang et al., 2014). A related approach is the factor-separation method, which for M sources involves analysis of a set of 2^M simulations (Stein and Alpert, 1993; Tao et al., 2005). Each simulation includes emissions from a different source or a different combination of sources. Pollutant concentrations are assigned not just to sources but to interactions among sources.

Another approach involves the use of reactive tracers for individual chemical species, sources, and/or geographic regions (Yarwood et al., 1996; Dunker et al., 2002b; Mysliwiec and Kleeman, 2002; Wagstrom et al., 2008; Wang et al., 2009; Grewe et al., 2010; Butler et al., 2011; Emmons et al., 2012; Kwok et al., 2013). However, various chemical assumptions (beyond those in the chemical mechanism) are needed to track production of the secondary pollutant in nonlinear reactions. In addition, the source contributions are often restricted to be positive even if some primary pollutants can inhibit formation of the secondary pollutant. Assignment methods trace through all the reaction pathways from products back to parent

reactants (Bowman and Seinfeld, 1994; Bowman, 2005). These methods also require extra chemical assumptions for reactions in which a product results from multiple reactants. Lastly, local sensitivity coefficients have been used to apportion ozone (O_3) and PM (Dunker et al. 2002b; Cohan et al., 2005; Koo et al., 2009). This approach involves constructing a Taylor series representation of the concentration as a function of source emissions and extrapolating the representation to zero emissions.

This work presents a new approach for source apportionment called the Path-Integral Method (PIM). The PIM provides a new, direct mathematical connection between sensitivity analysis and source apportionment and a connection between source apportionment and emission-control strategies. In contrast to reactive-tracer and assignment methods, the PIM does not require additional chemical assumptions. An important advantage of the PIM is its ability to allocate to sources a concentration increment, i.e., the difference between two simulations (base and background cases). If the anthropogenic increment is allocated to sources, the PIM requires that the base-case concentration minus the sum of the anthropogenic source contributions equals the background concentration. Other methods do not have this requirement, and thus may ascribe too much or too little importance to the anthropogenic sources. The PIM does require more computational effort than some other source apportionment methods because first-order sensitivities must be calculated at several levels of anthropogenic emissions.

The PIM is applied here to allocate the anthropogenic increments of O_3 and other species using a 2-cell configuration of the Comprehensive Air Quality Model with Extensions (CAMx) (ENVIRON, 2013). Another application of the PIM using a detailed, 3-D CAMx configuration for the eastern U.S. will be reported elsewhere (Dunker et al., 2015).

2 Description of the PIM

2.1 Equations

The PIM is based on an exact mathematical equation that is in itself not new. In particular, the equation is routinely used in thermodynamics (Sect. 2.3). However, the application of the equation to atmospheric modeling is new. The equation is the generalization to multiple variables of a familiar relationship for a single variable, namely that the integral of the

derivative of a function ($\int_a^b (df/dx)\ dx$) is equal to the difference in the value of the function at the ends of the integration interval (*f(b) – f(a)*).

For this work, the equation (Kaplan, 1959) takes the form

$$\Delta c_i(\boldsymbol{x},t) = c_i^1(\boldsymbol{x},t;\ \boldsymbol{\Lambda}=1) - c_i^0(\boldsymbol{x},t;\ \boldsymbol{\Lambda}=0) = \sum_{m=1}^{M} \int_P \frac{\partial c_i(\boldsymbol{x},t;\boldsymbol{\Lambda})}{\partial \lambda_m}\, d\lambda_m \qquad (1)$$

The c_i^1 is the concentration of species i in the base case, with all emissions present, and c_i^0 is the concentration in the background case, with *M* emission sources removed. $\boldsymbol{\Lambda}$ is the array of the parameters λ_m that scale the emissions of the *M* sources. If all $\lambda_m = 0$ ($\boldsymbol{\Lambda} = 0$), the emissions are those of the background case, and if all $\lambda_m = 1$ ($\boldsymbol{\Lambda} = 1$), the emissions are those of the base case. The $\partial c_i/\partial \lambda_m$ are the first-order sensitivities of c_i with respect to the scaling parameters. The integrals on the right side of Eq. (1) are taken over a curve or path *P* in *M*-dimensional space leading from the emissions in the background case to those in the base case. The Δc_i is the difference between the concentrations in the base and background cases at the same spatial location $\boldsymbol{x}$ and time *t*.

Although the focus here is on emissions, Eq. (1) can also include parameters that scale the initial and boundary concentrations. Furthermore, if the background case has all emissions and initial and boundary concentrations set to zero, then $c_i^0 = 0$ and Δc_i is the total concentration. Thus, the PIM can allocate the total concentration in a simulation as well as concentration differences between simulations.

The contribution of source m to Δc_i, S_{im}, is defined to be

$$S_{im}(\boldsymbol{x},t;P) = \int_P \frac{\partial c_i(\boldsymbol{x},t;\boldsymbol{\Lambda})}{\partial \lambda_m}\, d\lambda_m \qquad (2)$$

The PIM does not strictly require that the source contributions be calculated for all *M* sources or that Δc_i be calculated. The sensitivities can be determined for a subset of the sources and integrated to obtain the S_{im} only for the sources of interest. However, if all the source contributions and Δc_i are calculated, then Eq. (1) can be used to check the accuracy of the integration procedure. The integration procedure can be modified then, if necessary, so that the sum of the source contributions equals Δc_i within the desired error tolerance.

The source contributions depend on the path *P* from the point $\mathbf{\Lambda} = 0$ to the point $\mathbf{\Lambda} = 1$. Because there are an infinite number of paths between these two points, there are an infinite number of sets of source contributions, one set corresponding to each path. Viewed in the direction of integration, from $\mathbf{\Lambda} = 0$ to $\mathbf{\Lambda} = 1$, emissions are added into the background case until the base case is reached. Viewed in the opposite direction, emissions are controlled from the base case until the background case is reached. Thus, each path *P* represents a possible emission-control scenario, and the contribution of a given source to the change in concentration Δc_i depends on the control scenario.

Because the sensitivities are integrated over the path P in Eq. (2), the PIM considers a range of chemical conditions in calculating the source contributions, from zero to the full anthropogenic emissions in the base case. Methods based on tracers or a Taylor series expansion (e.g., with first- and second-order sensitivities) use only the emissions and the chemical conditions of the base case. Thus, the PIM provides source contributions that are averaged over the emission-control scenario, not specific to the base case.

The path *P* can be described via a path variable *u* that describes position along the path. Each λ_m is a function of u, such that as *u* varies from 0 to 1, each $\lambda_m(u)$ also varies from 0 to 1, and the path P defining the changes in anthropogenic emissions is traced from the background case to the base case in the M-dimensional space of the scaling parameters λ_m. However, *u* may not equal the normalized distance along *P*, denoted by *s*, and *s* can be useful in designing the numerical integration procedure because it is easier to understand the distribution of the integration points using *s*. The absolute distance *D* is related to *u* by

$$D(u) = \int_0^u \left[\sum_{m=1}^{M} \left(\frac{d\lambda_m}{du} \right)^2 \right]^{1/2} du \qquad (3)$$

Then, $s(u) = D(u)/D(1)$. Changing the integration variable from u to *s*, the source contribution becomes

$$S_{im}(\boldsymbol{x}, t; P) = \int_0^1 \left. \frac{\partial c_i(\boldsymbol{x}, t; \mathbf{\Lambda}))}{\partial \lambda_m} \right|_{\mathbf{\Lambda}=\mathbf{\Lambda}(s)} \frac{d\lambda_m}{ds} \, ds \qquad (4)$$

with

$$\frac{d\lambda_m}{ds} = \frac{d\lambda_m}{du}\frac{D(1)}{\left[\sum_{m=1}^{M}\left(\frac{d\lambda_m}{du}\right)^2\right]^{1/2}} \quad (5)$$

The sensitivity in Eq. (4) is evaluated along the specific path defined by $\mathbf{\Lambda}(s)$. Also, though the emissions are reduced along the path and the concentrations are determined in a simulation with the reduced emissions, the sensitivity of c_i is to λ_m, which scales the full emissions in the base case, not the reduced emissions. The decoupled direct method (DDM) provides an accurate, efficient means for calculating the sensitivities (Dunker, 1981, 1984; Yang et al., 1997). The DDM has been implemented in current 3-D models for the formation of O_3 and particulate matter (Dunker et al., 2002a; Cohan et al., 2005; Napelenok et al., 2006; Koo et al., 2007).

The simplest and shortest integration path, termed the diagonal path, is defined by $\lambda_m(u) = u$, all m. This is a straight line from $\mathbf{\Lambda} = 0$ to $\mathbf{\Lambda} = 1$ along which the emissions from all sources are reduced or grown by the common factor $\lambda_m(u) = u$. If there are two sources, Fig. 1 displays the diagonal path, Path 1, and two other possible paths. Path 2 is defined by the equations:

$$\lambda_1(u) = u^3 \quad (6)$$

$$\lambda_2(u) = \sin\left(\pi\frac{u}{2}\right) \quad (7)$$

Beginning at the base case, point B, emissions from source 1 are reduced much more rapidly than those from source 2 along Path 2. As the first 80% of the emissions from source 1 are reduced, only 20% of the emissions from source 2 are reduced. Then the remaining 80% of the emissions from source 2 are reduced as the remaining 20% of the emissions from source 1 are reduced, down to the background case, point b. Path 3 is the opposite of Path 2, obtained by interchanging the definitions of λ_1 and λ_2 in Eqs. (6, 7). For the diagonal path, the normalized distance and path variable are identical, $s(u) = u$, and $d\lambda_m/ds$ in Eq. (4) is identically 1. For Paths 2 and 3, $s(u) \neq u$, and $d\lambda_m/ds$ must be determined from Eq. (5).

The Gaussian numerical integration formulas have maximum precision (Isaacson and Keller, 1966). This means that for a given number of points at which the integrand is evaluated, n, the formulas give an exact integration of all polynomials of degree 0 up to $2n-1$, the maximum degree possible using n points. Thus, the Gaussian formulas should minimize the number of points at which the integrand in Eq. (4) must be evaluated to achieve a given accuracy. This is

useful because the major computational effort in the PIM is determining the sensitivities at multiple points along the path *P*. The Gauss-Legendre formula is one version of Gaussian integration suited to integration of a function *f(z)* over a finite interval:

$$\int_a^b f(z)dz \cong \frac{b-a}{2} \sum_{k=1}^{n} w(\xi_k)\, f\left(\frac{b-a}{2}\,\xi_k + \frac{b+a}{2}\right) \tag{8}$$

$$z = \frac{b-a}{2}\,\xi + \frac{b+a}{2} \tag{9}$$

The ξ_k are the zeroes of the Legendre polynomials, and the $w(\xi_k)$ are weights determined to give the formula the maximum precision. The ξ_k and $w(\xi_k)$ are readily available (efunda, 2014).

2.2 Special cases

One special case is successive zero-out (SZO) of the sources. In SZO, the emissions from one source are reduced to zero while leaving all other emissions unchanged, then the emissions from a second source are reduced to zero, etc. until the background case is reached. This is a path along the edges of a hypercube in **Λ**-space. (The hypercube defines all possible emission-control strategies, contains M axes, one axis for each λ_m, and includes all values of λ_m from 0 to 1.) In Fig. 1, one SZO path would be *B-b2-b* and the other, *B-b1-b*. Along the segment *B* to *b2* of the former path, the sensitivities are nonzero, but $d\lambda_2 = 0$. Therefore, the only contribution to Δc_i in Eq. (1) is that for source 1, and this contribution equals $c_i^B - c_i^{b2}$. Similarly, along the segment from *b2* to *b*, $d\lambda_1 = 0$, the only contribution to Δc_i is that for source 2, and the contribution equals $c_i^{b2} - c_i^b$. Thus, a SZO path is a special case of PIM in which no calculation or integration of sensitivities is required, only a series of simulations to obtain the concentrations at the corners of the hypercube. Calculation and integration of the sensitivities is necessary if two or more sources are controlled simultaneously, and the path is then interior to the hypercube.

Another special case involves expanding the sensitivities in a Taylor series in the λ_m at $\mathbf{\Lambda} = 1$ (base case). If there are two sources and the Taylor series through first order in λ_m is integrated along the diagonal path, then (see Supplementary Information (SI))

$$S_{i1}(diag) = \left.\frac{\partial c_i}{\partial \lambda_1}\right|_{\mathbf{\Lambda}=1} - \frac{1}{2}\left.\frac{\partial^2 c_i}{\partial {\lambda_1}^2}\right|_{\mathbf{\Lambda}=1} - \frac{1}{2}\left.\frac{\partial^2 c_i}{\partial \lambda_1 \partial \lambda_2}\right|_{\mathbf{\Lambda}=1} \quad (10)$$

$$S_{i2}(diag) = \left.\frac{\partial c_i}{\partial \lambda_2}\right|_{\mathbf{\Lambda}=1} - \frac{1}{2}\left.\frac{\partial^2 c_i}{\partial {\lambda_2}^2}\right|_{\mathbf{\Lambda}=1} - \frac{1}{2}\left.\frac{\partial^2 c_i}{\partial \lambda_1 \partial \lambda_2}\right|_{\mathbf{\Lambda}=1} \quad (11)$$

The cross term (- $\partial^2 c_i/\partial\lambda_1\partial\lambda_2$) is split evenly between S_{i1} and S_{i2}. If the integration is done instead on the path *B-b1-b* in Fig. 1, the full cross term is assigned to S_{i1} and is absent entirely from S_{i2}. Similarly, if the integration is along the path *B-b2-b*, the full cross term is assigned to S_{i2} and is absent from S_{i1}. Thus, the source contributions are the same for these 3 paths except for the location of the cross term. Cohan et al. (2005) expanded c_i in a second-order Taylor series about $\mathbf{\Lambda} = 1$ and used it to develop source apportionments that are the same as Eqs. (10, 11) except that they did not assign the cross term to the individual sources. The PIM shows that the cross term can be assigned to sources based on the emission-control path.

2.3 Analogy in thermodynamics

The dependence of the source contributions on path has an analogy in thermodynamics. For example, in the case of a single-component gas, the energy E is a function of the state variables: temperature T, and volume V. The change in E between two states of the system, ΔE, depends only on the initial and final values of T and V. However, when ΔE is split into contributions from the heat exchange with the surroundings ($\int_P dq$) and the pressure (p)-related work ($\int_P pdV$) in the equation, $\Delta E = \int_P dq - \int_P pdV$, the heat exchange and work depend on the path P from the initial to final states of the system. Thus, the concentrations c_i from an air quality simulation may be regarded as analogous to E and the emissions, initial and boundary concentrations, meteorology and chemical mechanism as analogous to T and V. The Δc_i between two simulations differing only in emissions can be allocated to sources, but this allocation is analogous to heat exchange and work and depends on the path along which the emissions are changed.

3 Model and inputs

Time-dependent inputs were developed for CAMx, v6.00, configured with 2 cells in a vertical column. The lower cell varied diurnally in height from 100 →300 →100 m and the upper cell varied in height such that the top of the column was 1500 m. Diurnally varying emissions were introduced at the bottom boundary. The simulations were run for 3 days, June 20-22, beginning with clean initial concentrations in both cells. There was no transport into the cells via the lateral or top boundaries. The latitude was that of Los Angeles and Atlanta. The Carbon Bond 6 (CB6) chemical mechanism represented the gas-phase chemistry (Yarwood et al., 2012). The effect of the inputs is that cleaner air from the upper cell is entrained into the lower cell during the morning as the lower cell grows in height. Then, in the evening, the lower cell shrinks in height and leaves pollutants aloft in the upper cell. Consequently, there is carry-over of pollutants from day to day affecting the chemistry in the lower cell. Additional details of the simulations are in Table S1 (SI).

The emissions were developed from the national totals in the 2008 U.S. National Emission Inventory, version 3 (U.S. EPA, 2013b) with several adjustments. Emissions from wildfires and prescribed fires were excluded because these vary greatly from year to year and were unusually high in 2008. Also, to represent summer conditions, emissions from residential wood combustion were excluded. Further, emissions of NO from lightning were added (Koo et al., 2010). The emissions were segregated into biogenic (plus lightning) emissions and 5 major source categories of anthropogenic emissions: fuel combustion, industrial sources, on-road vehicles, non-road vehicles, and other emissions. Vegetation and soil emissions and their speciation are from BEIS3.14 (Pierce et al., 1998). Anthropogenic emissions of volatile organic compounds (VOC's) from a major source category were allocated to CB6 species using speciation profiles from SPECIATE 4.3 for 1 or 2 sub-categories of sources comprising a significant fraction of the VOC emissions (Simon et al., 2010; U.S. EPA, 2013a). The annual emissions of VOC species, NOx (=NO + NO_2), CO, and HONO for each source category were allocated to hours of a Wednesday in June using temporal profiles (U.S. EPA, 2013c). On a national scale, the biogenic VOC emissions are large compared to the anthropogenic VOC emissions, but this is not the case in urban areas. To represent better an urban area the anthropogenic emissions were weighted by a factor of 5 and the biogenic emissions by a factor of 1. A summary of the resulting daily emission rates for all source categories is given in Table 1, and the complete set of emission rates is in Table S2.

The model and inputs are not intended to be a detailed representation of a specific urban area but rather to provide a useful platform for testing the PIM, specifically different integration formulas and the dependence of the source contributions on paths.

4 Results

The concentrations of O_3 and formaldehyde (FORM) in the background simulation (biogenic emissions only), the base simulation (both the biogenic and anthropogenic emissions) and the difference between the simulations (anthropogenic increment) are shown in Fig. 2. Similar plots for NO_2 and HNO_3 are in Fig. S1. The peak O_3 concentration remains relatively constant over the 3 days in the background simulation (47-52 ppb) but increases steadily in the base simulation (from 75 ppb on day 1 to 151 ppb on day 3) due to the additional anthropogenic emissions on days 2 and 3 and the carryover of pollutants in the upper cell. Both O_3 and FORM have sizeable concentrations in the background case whereas NO_2 and HNO_3 have very low concentrations due to the low biogenic NO_x emissions. The O_3 increment is negative at the beginning of day 1 due to the titration of O_3 by the anthropogenic NO emissions. The VOC/NO_x ratio in the base case increases from 5-7 on day 1 to 9-20 ppbCppb^{-1} on day 3. Overall, the simulations provide a wide range of conditions for testing the PIM.

4.1 Accuracy of the numerical integration

The O_3, FORM, NO_2, and HNO_3 increments were allocated to the 5 anthropogenic source categories and to the 4 species or groups of species emitted by each source category: VOC, CO, NO_x, and HONO. Thus, a total of $M = 20$ sensitivities were calculated and integrated in the PIM. Source apportionments were determined for 3 emission-control paths: diagonal (Diag); VOC first (VOCF); NO_x first (NOxF). Along the Diag path, the scaling parameters $\lambda_m^{VOC} = \lambda_m^{CO} = \lambda_m^{NOx} = \lambda_m^{HONO} = u$, for each source category $m = 1, \ldots, 5$. Thus, the sources and emission species are treated equivalently. The VOCF path emphasizes initial control of VOC and CO emissions followed by later control of NO_x and HONO emissions, as defined by $\lambda_m^{VOC} = \lambda_m^{CO} = u^3$ and $\lambda_m^{NOx} = \lambda_m^{HONO} = \sin(\pi u/2)$, $m = 1, \ldots, 5$. The NOxF path has the reverse assignments of u^3 and $\sin(\pi u/2)$. Viewing λ_m^{VOC}, λ_m^{CO} as analogous to λ_1 in Fig. 1 and λ_m^{NOx}, λ_m^{HONO} as analogous to λ_2, , then the VOCF path in 20-dimensional space is analogous to Path 2 in Fig. 1 and the NOxF path is analogous to Path 3.

The Gauss-Legendre formula was tested for accuracy using different numbers of integration points and different integration variables. One set of tests, labeled GLns, used the distance *s* as the integration variable and *n* integration points. Another set of tests, labeled GLnr, used a transformation of the variable *s* to $r = s^{1/2}$. Equation (4) then becomes

$$S_{im}(\boldsymbol{x}, t; P) = 2 \int_0^1 \left. \frac{\partial c_i(\boldsymbol{x}, t; \boldsymbol{\Lambda}))}{\partial \lambda_m} \right|_{\boldsymbol{\Lambda}=\boldsymbol{\Lambda}(s[r])} \left. \frac{d\lambda_m}{ds} \right|_{s(r)} r \, dr \tag{12}$$

Because the background case contains no anthropogenic emissions, O_3 formation is strongly limited by the availability of NO_x. As a consequence, the sensitivity of O_3 with respect to any λ_m that scales NO_x emissions is very large near $\boldsymbol{\Lambda} = 0$, but the sensitivity decreases very rapidly as NO_x emissions are added. The transformation to *r* has two potentially beneficial effects for the source apportionment of O_3. First, the points for the numerical integration are chosen for the variable *r*. When transformed back to the variable *s*, the points for *s* are closer to $\boldsymbol{\Lambda} = 0$ than if *s* were the integration variable, giving more resolution where the sensitivity is changing most rapidly. Second, the factor *r* in Eq. (12) reduces the magnitude of the integrand near $r = s = \lambda_m = 0$, and makes the integrand identically 0 at $r = 0$. This can yield an integrand that is easier to integrate. Finally, as a simple alternative, the source contributions were calculated by the trapezoidal rule using the 2 points at $\boldsymbol{\Lambda} = 0$ and 1 (labeled TR2).

The sum of the source contributions on the 3 paths was compared to the anthropogenic concentration increment (right- vs. left-hand sides of Eq. (1)) to determine the accuracy of the formulas. Table 2 gives the mean absolute error and mean bias of the formulas for O_3 and FORM, and Table S3 gives the error and bias for NO_2 and HNO_3. For comparison, the mean absolute values of the increments ΔO_3, ΔFORM, ΔNO_2, and ΔHNO_3 are 34.9 ppb, 1.52 ppb, 7.67 ppb, and 16.0 ppb, respectively. Though they use the same number of points, there is a large reduction in error and bias from TR2 to GL2s or GL2r, indicating the significant advantage of the GL formulas. As the number of points included in the GLns or GLnr formulas increases, the error decreases for O_3, FORM, and NO_2 and generally the bias as well. There are some exceptions to this trend for HNO_3, but these occur for cases where the error and bias are already quite low (average error < 4% of the average increment). For O_3 and the Diag path, the GLnr formula gives more accurate results than the GLns formula for 2 or 3 points and essentially the same accuracy for 4 points. For FORM, the GLnr formula is always more

accurate than the GLns formula. The GLnr formula is usually less accurate than the GLns formula for NO_2 and HNO_3 and for O_3 with the NOxF and VOCF paths.

Table 2 also shows that the accuracy of a formula is lower for the VOCF path than the other paths when using the same number of points. This difference can be understood by examining the integrand in Eq. (4). Figure 3 displays the integrands for allocating ΔO_3 to sources at the time of peak O_3 on day 3, when it is most difficult to obtain good agreement between the sum of the source contributions and ΔO_3. Along the Diag and NOxF paths, the integrands have a constant curvature, either positive (Diag) or negative (NOxF), and the integrands are mainly positive, with only small negative values near $s = 1$. However, along the VOCF path, 4 of the integrands have positive curvature from $s = 0$ to $s = \sim 0.5$ and then negative curvature for the remainder of the path. Also, the integrands vary over a wider range along the VOCF path than the other paths. Further, the integrands for on-road vehicles and fuel combustion are both positive and negative, resulting in the cancellation of contributions to the integrals from different sections of the path. The change in curvature, wider range of variation and especially the cancellation of contributions require more points on the VOCF path to obtain an accurate integration.

Overall, the GL3r formula for the Diag path and the GL4s formula for the other paths give quite accurate results and were used to calculate the source apportionments in Sect. 4.2. Figure S2 gives a comparison of the sum of the source contributions vs. ΔO_3, ΔFORM, ΔNO_2, and ΔHNO_3 at each hour of the simulation. The plots show again that the largest errors occur for the VOCF path.

4.2 Source apportionments

Figure 4 presents the apportionment of ΔO_3 to the 5 source categories and 4 emission species using the Diag path. The VOC contributions are always positive, and the largest contributions are from industrial sources and on-road and non-road vehicles. The NO_x contributions are small and primarily negative on day 1, when the atmospheric VOC/NO_x < 7.5 ppbCppb^{-1} in the base case. Under these conditions, NO_x emissions tend to inhibit O_3 formation, and hence the contributions are negative. On day 2, however, the NO_x contributions become positive and then increase from day 2 to day 3. The total of the NO_x contributions from all sources at 42 h is essentially the same as the total VOC contribution, and at 66 h, the total NO_x contribution is twice the total VOC contribution. The increasing importance of the NO_x contributions is due

to the increasing VOC/NO_x, which is 10-20 ppbCppb^{-1} after 36 h, resulting in NO_x-limited O_3 formation.

The PIM can separate the contributions of all emission species. Figure 4 shows that the CO contributions from on-road and non-road vehicles are not negligible compared to the VOC contributions of these sources. For on-road vehicles, the CO contributions are generally 20-45% of the VOC contributions, and for non-road vehicles, 10-30%. HONO emissions are assigned only to on-road and non-road vehicles and are small (0.8% of NO_x, Table 1). For both of these sources, their HONO emissions contribute < 0.35 ppb to the ΔO_3.

Figure 5 displays the source contributions to ΔO_3 obtained with the 3 paths. (The contributions of all emission species from a source are combined together.) Results for the Diag and NOxF path are similar. For these paths, on-road vehicles have the largest and non-road vehicles the second-largest contributions during most of the simulation, and the "other" category contributes <3 ppb to ΔO_3. However, industrial sources are more important than fuel combustion for the Diag path and the reverse is true for the NOxF path. The source contributions for the VOCF path are distinctly different. Over most of the simulation, the ranking of the contributions is industrial sources > non-road vehicles > on-road vehicles, the opposite of the Diag path. Also, fuel combustion has a negative contribution over the entire simulation and the other category has a larger contribution (up to 6.5 ppb) than for the Diag and NOxF paths.

The different results for the VOCF path can be explained by the fact that the NO_x emissions are controlled last on this path or, in terms of the integration, essentially only NO_x emissions are added near $s = 0$. The sensitivity of O_3 to these emissions is large and positive near $s = 0$ (Fig. 3) because the VOC/NO_x ratio is high in the background case. However, the VOC/NO_x ratio decreases rapidly as s increases along the VOCF path, the sensitivity to NO_x emissions becomes negative, and O_3 formation becomes VOC-limited for most of the path. Thus, fuel combustion has a negative source contribution because its emissions are mostly NO_x, and industrial sources have the largest positive contribution because they have the largest VOC emissions. Also, non-road vehicles have a larger contribution than on-road vehicles because both sources have a similar magnitude of VOC emissions but on-road vehicles have 82% more NO_x emissions, which suppress O_3 formation on the VOC-limited section of the path.

The source contributions to ΔFORM for the 3 paths are also in Fig. 5. For the Diag path, the relative importance of the sources on days 2 and 3 is the same for ΔFORM as for ΔO_3, and this is also true for the NOxF path. For the VOCF path, the on-road and non-road vehicles

contribute more to ΔFORM than the industrial sources, but the reverse is true for the contributions of these sources to ΔO_3. The on-road and non-road vehicles have the largest contributions to ΔFORM on each path because these sources have the largest primary FORM emissions and the largest emissions of olefins, which are important precursors to secondary FORM from oxidation reactions (Table S2).

Figure S3 contains the apportionment of ΔNO_2 and ΔHNO_3 to sources. The source contributions to ΔNO_2 for the Diag and NOxF paths are quite similar; those for the VOCF path differ in that the contributions of the industrial sources and other category are primarily negative after 18 h. The source contributions to ΔHNO_3 for the Diag and NOxF paths are again quite similar, and the ranking of the sources in importance is the same as the ranking of their NO_x emissions. The source contributions to ΔHNO_3 for the VOCF path are similar to those for the other paths except that the contributions of non-road vehicles and fuel combustion are reversed in importance. The reversal is likely due to the much larger VOC emissions from non-road vehicles, which would enhance the oxidation of NO_x on the VOC-limited part of the path.

5 Conclusions

As shown in Sect. 4, the PIM can allocate the difference in concentration between two simulations to emission sources. Consequently, the PIM requires that the base-case concentration minus the sum of the anthropogenic source contributions (difference δ) equals the background concentration (within the accuracy of the numerical integration). Other methods do not have this constraint. If δ is less than the background concentration, then the method assigns too much importance to the anthropogenic sources and will give the impression that reducing anthropogenic emissions will reduce the pollutant concentration more than will actually occur (over-allocation of the anthropogenic increment to the anthropogenic sources). Similarly, if δ is greater than the background concentration, the method assigns too little importance to the anthropogenic sources (under-allocation of the anthropogenic increment). The PIM ensures that the anthropogenic increments to O_3 and the other species are neither over- nor under-allocated to the anthropogenic sources.

Another advantage is that the PIM is based on an exact mathematical relationship that is independent of the chemistry or model and does not require added relationships or approximations. The PIM allows source contributions to be either positive or negative. If the

secondary pollutant formation is inhibited by emissions of some species, source, or geographic area, the sensitivity to these emissions will be negative for at least some values of the scaling parameter λ_m, and the integral in Eq. (2) may be negative.

Once a model has been modified to calculate the first-order sensitivities, the PIM requires only very simple post-processing of model results, specifically, calculating a linear combination of sensitivities from different simulations. This can be readily done with existing post-processing packages such as the Package for Visualization of Environmental data (PAVE) or the Visualization Environment for Rich Data Interpretation (VERDI) (Univ. of North Carolina, 2004, 2014). The PIM is not focused on just one species, e.g., O_3. The calculations needed to allocate Δc_i for species i also generate all the information needed to allocate Δc_j for any other species j predicted by the model, and there is minimal additional effort needed to allocate Δc_j for the second and subsequent species. Finally, the PIM highlights the importance of the background simulation. For a simulation with anthropogenic emissions included to be useful in designing emission controls, there is an implicit assumption that a simulation without the anthropogenic emissions gives concentrations consistent with estimates for clean air. The concentration in the background simulation can be determined by an actual simulation or by subtracting the sum of all the source contributions from the base-case concentration.

In principle, there is an infinite number of source apportionments available from the PIM. However, each source apportionment is linked to an emission-control strategy. If a control strategy is defined along with the timing of the controls, the number of source apportionments is reduced to just one.

The major disadvantage of the PIM is that it requires more computational effort than other methods because the sensitivities must be determined at several emission levels between the base and background simulations. This disadvantage is mitigated, to some degree, because the additional simulations provide information on how concentrations and sensitivities will change along the emission-control path.

The PIM has been applied in this work to a simplified configuration of CAMx that includes the nonlinear chemistry but not transport or dispersion. However, transport and dispersion do not involve nonlinear interactions among the species. Because the nonlinear dependence of the sensitivities on the integration variable (Fig. 3) is driven by the nonlinear chemistry and a full 3-D configuration should not have any other sources of nonlinearity, the number of integration

points required for PIM for a 3-D configuration should be similar to the number required for the simplified configuration (3 or 4) (Dunker et al., 2015).

Supplementary information

Application of the PIM to the special case involving the Taylor series expansion, input data and emissions for the model simulations, accuracy in allocating ΔNO_2 and ΔHNO_3 to sources using different integration formulas, comparison of the sum of the source contributions to the anthropogenic increment at each hour, and source contributions to ΔNO_2 and ΔHNO_3.

References

Bowman F. M.: A multi-parent assignment method for analyzing atmospheric chemistry mechanisms, Atmos. Environ., 39, 2519-2533, 2005.

Bowman, F. M. and Seinfeld, J. H.: Ozone productivity of atmospheric organics. J. Geophys. Res., 99, 5309-5324, 1994.

Butler, T. M., Lawrence, M. G., Taraborrelli, D., and Lelieveld, J.: Multi-day ozone production potential of volatile organic compounds calculated with a tagging approach, Atmos. Environ., 45, 4082-4090, 2011.

Cohan D. S., Hakami A., Hu, Y., and Russell A. G.: Nonlinear response of ozone to emissions: source apportionment and sensitivity analysis, Environ. Sci. Technol., 39, 6739-6748, 2005.

Dunker, A.M.: Efficient calculation of sensitivity coefficients for complex atmospheric models. Atmos. Environ., 15, 1155-1161, 1981.

Dunker, A. M.: The decoupled direct method for calculating sensitivity coefficients in chemical kinetics, J. Chem. Phys., 81, 2385-2393, 1984.

Dunker, A. M., Yarwood, G., Ortmann, J. P., and Wilson, G. M.: The decoupled direct method for sensitivity analysis in a three-dimensional air quality model- implementation, accuracy, and efficiency, Environ. Sci. Technol., 36, 2965-2976, 2002a.

Dunker, A. M., Yarwood, G., Ortmann, J. P., and Wilson, G. M.: Comparison of source apportionment and source sensitivity of ozone in a three-dimensional air quality model, Environ. Sci. Technol., 36, 2593-2964, 2002b.

Dunker, A. M., Koo, B., and Yarwood, G.: Source apportionment of the anthropogenic increment to ozone, formaldehyde, and nitrogen dioxide by the path-integral method in a 3-D model, submitted for publication, 2015.

efunda: available at http://www.efunda.com/math/num_integration/findgausslegendre.cfm (last access: 29 January 2014), 2014.

Emmons, L. K., Hess, P. G., Lamarque, J.-F., and Pfister , G. G.: Tagged ozone mechanism for MOZART-4, CAM-chem and other chemical transport models, Geosci. Model Dev., 5, 1531-1542, 2012.

ENVIRON: Comprehensive Air Quality Model with Extensions, available at; http://www.CAMx.com (last access: 15 May 2013), 2013.

Grewe, V., Tsati, E., and Hoor, P.: On the attribution of contributions of atmospheric trace gases to emissions in atmospheric model applications, Geosci. Model Dev., 3, 487-499, 2010.

Isaacson, E. and Keller, H. B.: Analysis of Numerical Methods, John Wiley, New York, 1966.

Kaplan, W.: Advanced Calculus, Addison-Wesley, Reading, Massachusetts, 1959.

Koo, B., Dunker, A. M., and Yarwood, G.: Implementing the decoupled direct method for sensitivity analysis in a particulate matter air quality model, Environ. Sci. Technol., 41, 2847-2854, 2007.

Koo, B., Wilson, G. M., Morris, R. E., Dunker, A. M., and Yarwood, G.: Comparison of source apportionment and sensitivity analysis in a particulate matter air quality model, Environ. Sci. Technol., 43, 6669-6675, 2009.

Koo, B., Chien, C.-J., Tonnesen, G., Morris, R., Johnson, J., Sakulyanontvittaya, T., Piyachaturawat, P., and Yarwood, G.: Natural emissions for regional modeling of background ozone and particulate matter and impacts on emissions control strategies, Atmos. Environ. 44, 2372-2382, 2010.

Kwok, R. H. F., Napelenok, S. L., and Baker, K. R.: Implementation and evaluation of PM2.5 source contribution analysis in a photochemical model, Atmos. Environ., 80, 398-407, 2013.

Marmur, A., Park, S.-K., Mulholland, J. A., Tolbert, P. E., and Russell, A. G.: Source apportionment of PM2.5 in the southeastern United States using receptor and emissions-based models: conceptual differences and implications for time-series health studies, Atmos. Environ., 40, 2533-2551, 2006.

Mysliwiec, M. J. and Kleeman M. J.: Source apportionment of secondary airborne particulate matter in a polluted atmosphere, Environ. Sci. Technol., 36, 5376-5384, 2002.

Napelenok, S. L., Cohan D. S., Hu, Y., and Russell A. G.: Decoupled direct 3D sensitivity analysis for particulate matter (DDM-3D/PM), Atmos. Environ., 40, 6112-6121, 2006.

Pierce, T., Geron, C., Bender, L., Dennis, R., Tonnesen, G., and Guenther, A.: Influence of increased isoprene emissions on regional ozone modeling, J. Geophys. Res., 103, 25611-25629, 1998.

Simon, H., Beck, L., Bhave, P.V., Divita, F., Hsu, Y., Luecken, D., Mobley, J.D., Pouliot, G.A., Reff, A., Sarwar, G., and Strum, M.: The development and uses of EPA's SPECIATE database, Atmospheric Pollution Research, 1, 196-206, 2010.

Stein, U. and Alpert, P.: Factor separation in numerical simulations, J. Atmos. Sci., 50, 2107-2115, 1993.

Tao, Z., Larson S. M., Williams A., Caughey, M. and Wuebbles D. J.: Area, mobile, and point source contributions to ground level ozone: a summer simulation across the continental USA, Atmos. Environ., 39, 1869-1877, 2005.

Tong, D. Q. and Mauzerall, D. L.: Summertime state-level source-receptor relationships between nitrogen oxides emissions and surface ozone concentrations over the continental United States, Environ. Sci. Technol., 42, 7976-7984, 2008.

University of North Carolina, Package for Analysis and Visualization of Environmental Data, version 2.3, available at: http://www.ie.unc.edu/cempd/EDSS/pave_doc/EntirePaveManual.html (last access: 17 November 2014), 2004.

University of North Carolina, Visualization Environment for Rich Data Interpretation, version 1.5, available at: https://www.cmascenter.org/verdi/ (last access: 17 November 2014), 2014.

U.S. EPA: Carbon Bond and SAPRC Speciation Profiles, available at: http://www.cmascenter.org/download/data.cfm (last access: 19 November 2013), 2013a.

U.S. EPA: 2008 National Emissions Inventory, Version 3, Technical Support Document, September 2013-Draft, available at: http://www.epa.gov/ttn/chief/net/2008inventory.html (last access: 20 November 2013), 2013b.

U.S. EPA: CAIR Platform Data, available at: http://www.epa.gov/ttn/chief/emch/temporal/index.html (last access: 24 December 2013), 2013c.

Wagstrom, K. M., Pandis, S. N., Yarwood, G., Wilson, G. M. and Morris, R. E.: Development and application of a computationally efficient particulate matter apportionment algorithm in a three-dimensional chemical transport model, Atmos. Environ., 42, 5650-5659, 2008.

Wang, H., Jacob, D. J., LeSager, P., Streets, D. G., Park, R. J., Gilliland, A. B., and van Donkelaar, A.: Surface ozone background in the United States: Canadian and Mexican pollution influences, Atmos. Environ., 43, 1310-1319, 2009.

Wang, Z. S., Chien, C. J. and Tonnesen, G. S.: Development of a tagged species source apportionment algorithm to characterize three-dimensional transport and transformation of precursors and secondary pollutants, J. Geophys. Res., 114, D21206, doi: 10.1029/2008JD010846, 2009.

Yang, Y-J., Wilkinson, J. G. and Russell, A. G.: Fast, direct sensitivity analysis of multidimensional photochemical models, Environ. Sci. Technol., 31, 2859-2868, 1997.

Yarwood, G., Morris, R. E., Yocke, M. A., Hogo, H. and Chico, T. Development of a methodology for source apportionment of ozone concentration estimates from a photochemical grid model, in: Proceedings of the 89th Annual Meeting of the Air & Waste Management Association, Air and Waste Management Association, Pittsburgh, PA, Paper 96-TA23A.06, 1996.

Yarwood, G., Gookyoung H., Carter, W.P.L., and Whitten, G.Z.: Environmental Chamber Experiments to Evaluate NO_x Sinks and Recycling in Atmospheric Chemical Mechanisms, Texas Air Quality Research Program Project 10-042, University of Texas, Austin, 2012.

Zhang, Y., Wang, W., Wu, S.-Y., Wang, K., Minoura, H. and Wang, Z. Impacts of updated emission inventories on source apportionment of fine particle and ozone over the southeastern U.S., Atmos. Environ., 88, 133-154, 2014.

1 Table 1. Summary of daily emission rates used in the base-case simulation.

Species	Emission Rate (mol day^{-1} km^{-2})					
	Biogenic Sources[a]	Fuel Combustion	Industrial Sources	On-road Vehicles	Non-road Vehicles	Other Sources
NO	13.5	77.4	19.7	132.9	73.2	1.9
NO2	0.00	8.60	2.19	13.59	7.48	0.21
HONO	0.00	0.00	0.00	1.18	0.65	0.00
CO	35.9	51.8	58.2	1158.4	683.0	57.0
VOC	166.8	6.1	244.3	129.9	115.1	59.3
VOC/NO_x[b]	29.8	0.09	16.6	1.4	2.4	31.8

2 [a] Includes lightning

3 [b] $NO_x = NO + NO_2$. VOC/NO_x units are mole C (mole NO_x)$^{-1}$

4

Table 2. Average error and bias for different numerical integration formulas. The sum of the source contributions calculated using the formula is compared to the anthropogenic increment of O_3 or FORM.

Path	Formula[a]	Mean Absolute Error[b] (ppb)	Mean Bias[b] (ppb)
		O_3 Increment	
Diag	TR2	65.93	65.93
Diag	GL2s	7.38	-7.36
Diag	GL2r	5.95	5.71
Diag	GL3s	3.32	-3.30
Diag	GL3r	1.64	-1.49
Diag	GL4s	1.51	-1.50
Diag	GL4r	1.54	-1.49
NOxF	GL3s	2.20	2.15
NOxF	GL3r	7.73	-7.67
NOxF	GL4s	1.57	-1.54
VOCF	GL3s	7.56	-7.32
VOCF	GL3r	10.46	9.62
VOCF	GL4s	4.68	-4.63
		FORM Increment	
Diag	TR2	2.45	2.45
Diag	GL2s	0.21	-0.20
Diag	GL2r	0.19	0.19
Diag	GL3s	0.12	-0.12

Diag	GL3r	0.04	0.02
Diag	GL4s	0.05	-0.04
Diag	GL4r	0.03	-0.02
NOxF	GL3s	0.11	-0.10
NOxF	GL3r	0.08	-0.01
NOxF	GL4s	0.08	0.08
VOCF	GL3s	0.30	-0.30
VOCF	GL3r	0.17	0.11
VOCF	GL4s	0.09	-0.08

[a] TR2 = trapezoidal rule, 2 points. GLnx = Gauss-Legendre formula using *n* points and *x* as the integration variable.

[b] Hourly average over the 3-day simulation.

Figure captions

Figure 1. Three possible integration paths when the concentration difference between the base (point B) and background (point b) cases is allocated to two sources with emissions scaled by λ_1 and λ_2. Path 1: equal control of emissions from both sources (diagonal path). Path 2: emphasis on control of emissions from source 1 first followed by control of emissions from source 2. Path 3: opposite of Path 2. Points b1 and b2 have the emissions from the background case plus source 1 and source 2, respectively.

Figure 2. Results from the 2-cell model simulations. Ozone and formaldehyde concentrations for the base case and the background case and the difference between them (anthropogenic increment).

Figure 3. Dependence of the integrands for allocating O_3 to sources on the distance *s* along the Diag, NOxF and VOCF paths. The integrand (Eq. (4)) is calculated at the time of peak O_3 on day 3 (66 h).

Figure 4. Contributions of sources and VOC, NO_x, CO, and HONO emissions to the anthropogenic O_3 increment. Results are for the Diag path.

Figure 5. Apportionment of the anthropogenic O_3 increment (left) and the FORM increment (right) to sources using the Diag, NOxF, and VOCF emission-control paths.

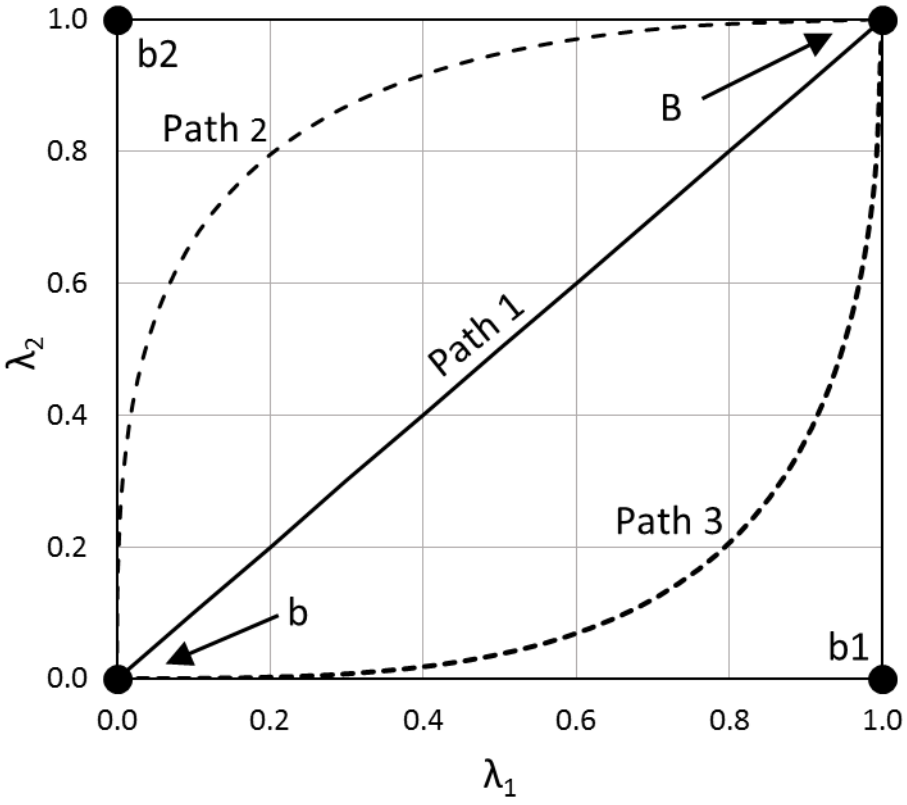

Figure 1. Three possible integration paths when the concentration difference between the base (point B) and background (point b) cases is allocated to two sources with emissions scaled by λ_1 and λ_2. Path 1: equal control of emissions from both sources (diagonal path). Path 2: emphasis on control of emissions from source 1 first followed by control of emissions from source 2. Path 3: opposite of Path 2. Points b1 and b2 have the emissions from the background case plus source 1 and source 2, respectively.

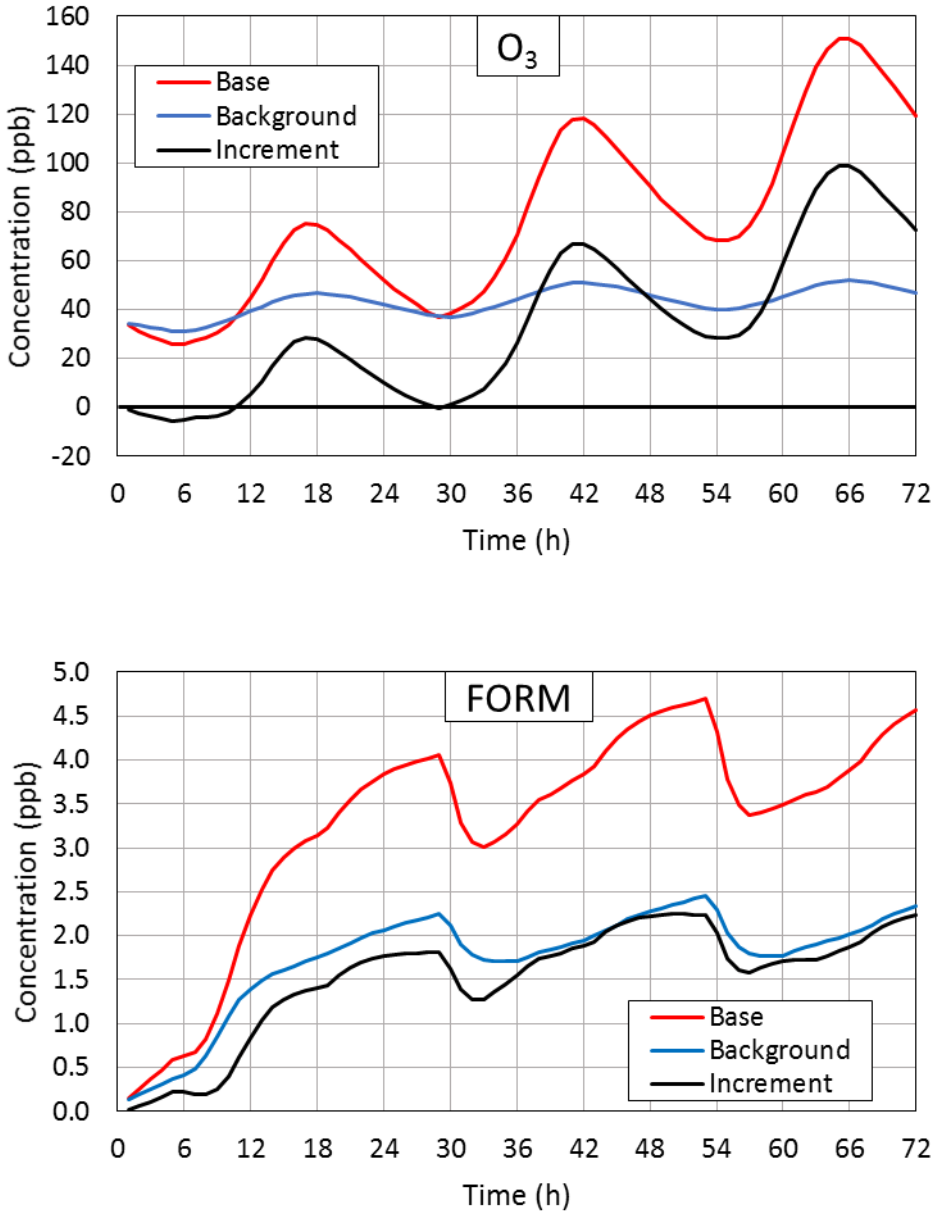

Figure 2. Results from the 2-cell model simulations. Ozone and formaldehyde concentrations for the base case and the background case and the difference between them (anthropogenic increment).

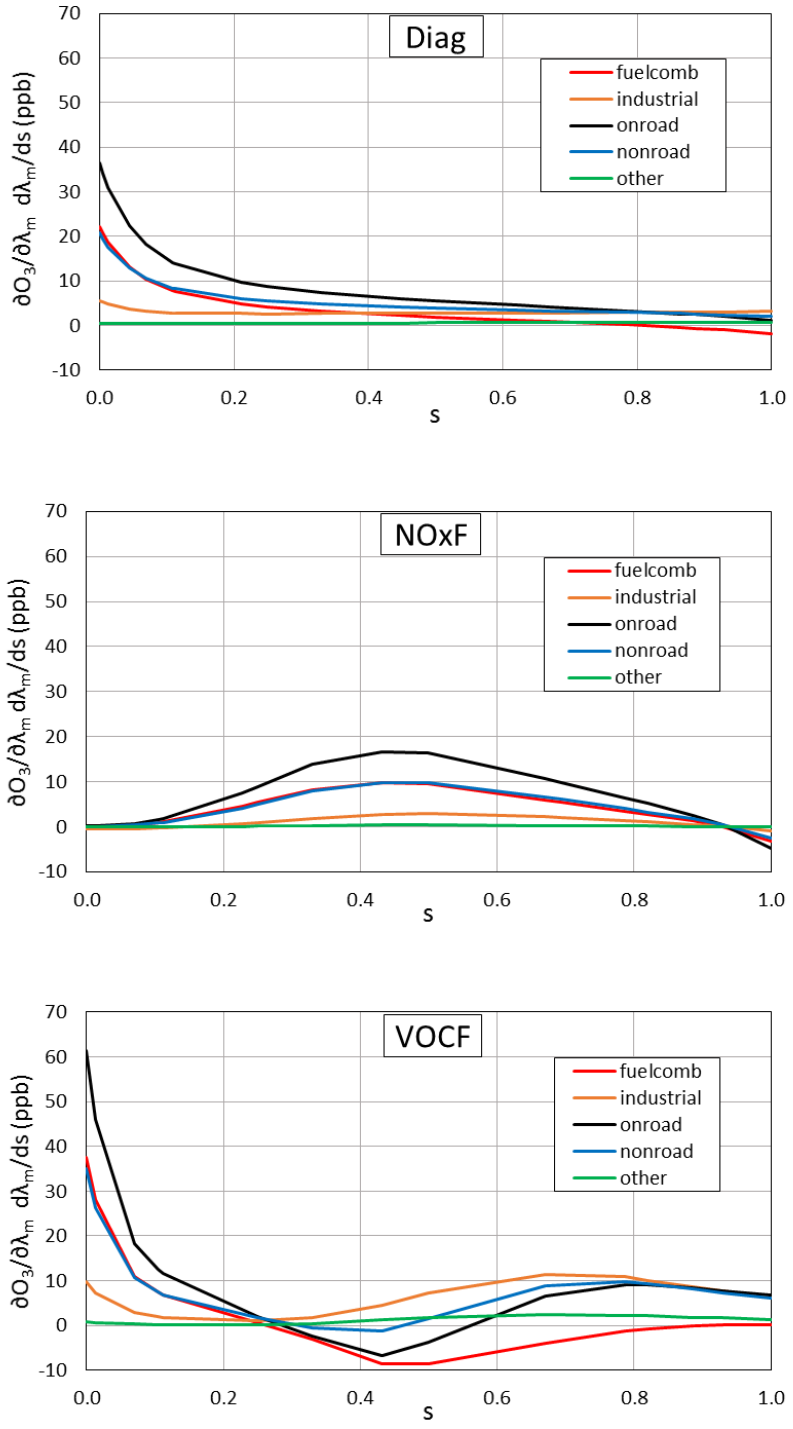

1

2 Figure 3. Dependence of the integrands for allocating O_3 to sources on the distance *s* along the
3 Diag, NOxF and VOCF paths. The integrand (Eq. (4)) is calculated at the time of peak O_3 on
4 day 3 (66 h).

5

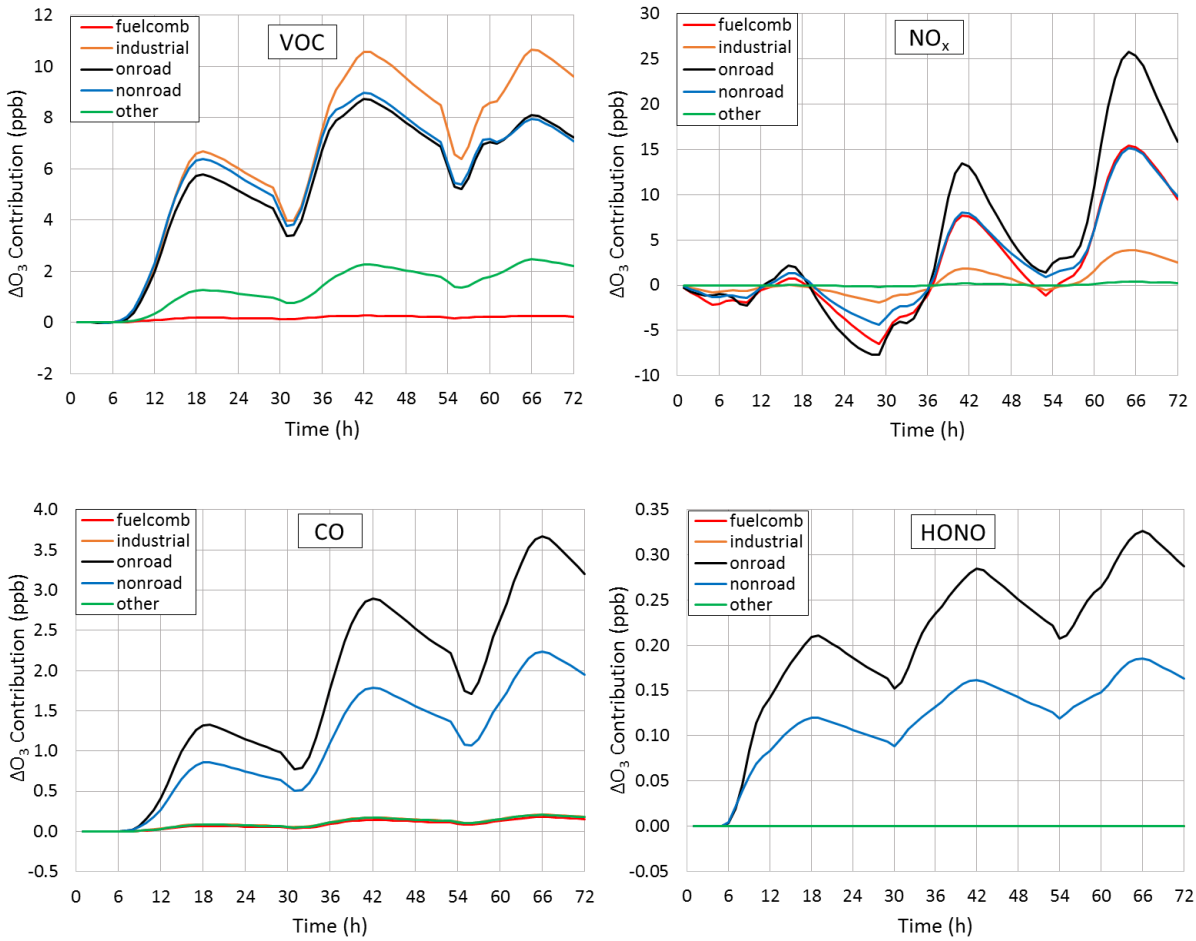

1

2 Figure 4. Contributions of sources and VOC, NO_x, CO, and HONO emissions to the
3 anthropogenic O_3 increment. Results are for the Diag path.

4

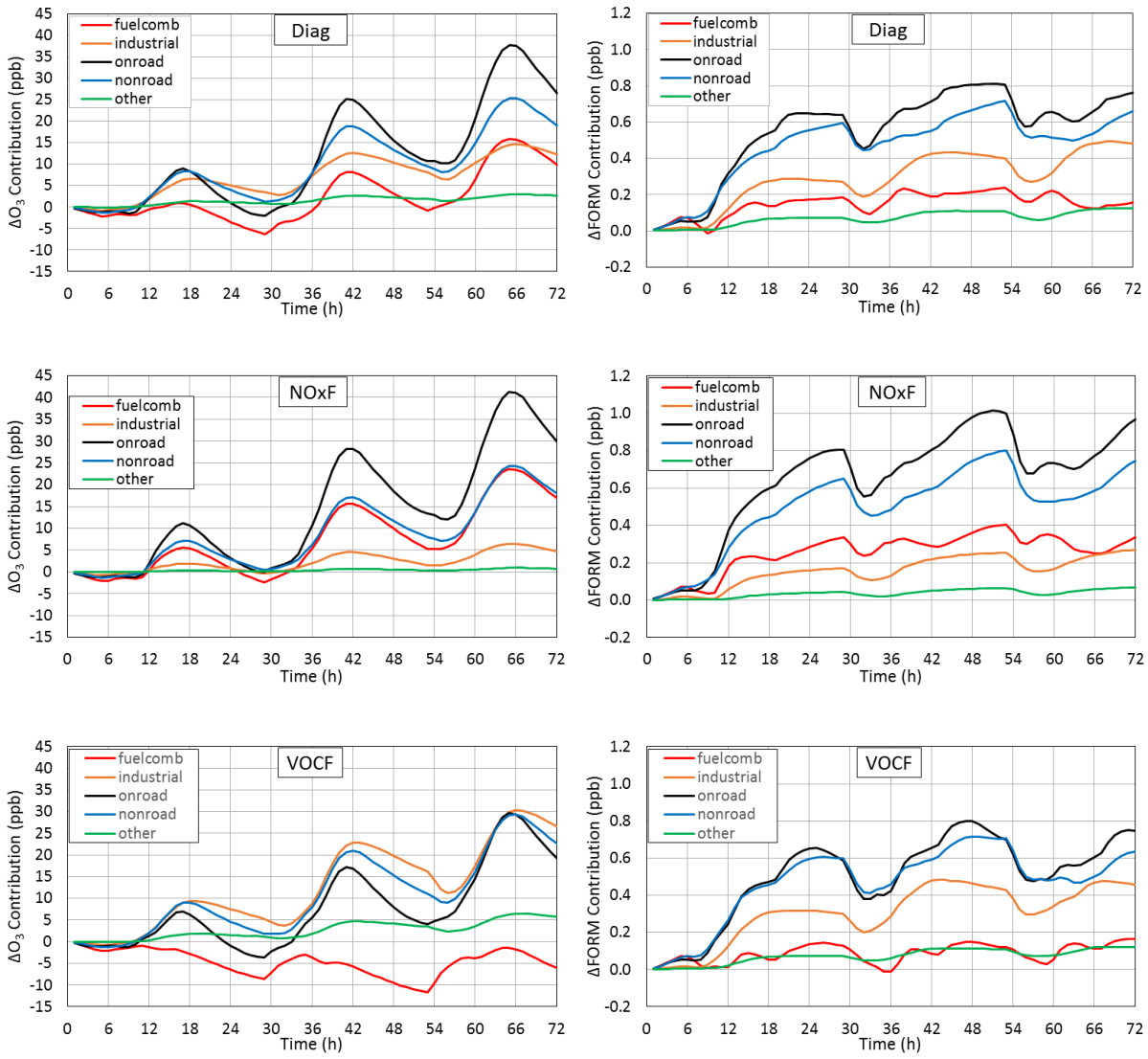

1

2 Figure 5. Apportionment of the anthropogenic O_3 increment (left) and the FORM increment
3 (right) to sources using the Diag, NOxF, and VOCF emission-control paths.